

Analysis of vessel induced erosion through manoeuvre simulation and AIS data

TONI LLULL

Maritime Engineering Laboratory, Department of Nautical Science and Engineering, UPC-Barcelona Tech.

e-mail: antoni.llull.marroig@upc.edu (author for correspondence)

JORDI MONCUNILL

Department of Nautical Science and Engineering, UPC-Barcelona Tech.

e-mail: jordi.moncunill@upc.edu

MARCELLA CASTELLS-SANABRA

Department of Nautical Science and Engineering, UPC-Barcelona Tech.

e-mail: marcella.castells@upc.edu

ANNA MUJAL-COLILLES

Maritime Engineering Laboratory, Department of Nautical Science and Engineering, UPC-Barcelona Tech.

e-mail: anna.mujal@upc.edu

XAVIER GIRONELLA

Maritime Engineering Laboratory, Department of Civil and Environmental Engineering, UPC-Barcelona Tech.

e-mail: xavi.gironella@upc.edu

ACKNOWLEDGMENTS

The authors wish to thank the Infrastructure and Conservation Division and the Port Operations and Planning Division of the Barcelona Port Authority for the bathymetric data provided and the recommendations about ship manoeuvring in the study basin.

Keywords

Propeller induced scour; Ship manoeuvre; AIS data; numerical simulator

Abstract

This manuscript presents an erosion induced by manoeuvring ships assessment methodology in harbour basins with low bed clearance conditions. From the evolution of the bottom morphology, obtained from bathymetric surveys performed by the Port Authority, AIS data is used to analyse the traffic patterns in the basin and to relate the particular ships manoeuvres with the bottom morphology evolution. This allows for the detection of ships causing higher erosion in the basin. The manoeuvre simulator yields the use of the engines and thrusters during the in-port manoeuvres. Afterwards, literature equations are used to perform a stability assessment of the bottom material allowing to

compute the required size for a rock protection layer in the basin.

1. INTRODUCTION

Common guidelines in the field of maritime engineering such as (BAW, 2010), (Puertos del Estado, 2012) or (PIANC, 2015) propose different prevention and protection systems against the scour induced by propellers in the navigation channel and the harbour basin. Predictive formulas are based on previous estimation of the efflux velocity (U_o) and the bed velocity (U_b), using different stability criteria as the threshold for the sediment resuspension. As reported by (Mujal-Colilles et al., 2017), most of the existing equations to compute the maximum scour depth overestimate real results of maximum scouring depth. However, the methods to design bed protections that are proposed in the previously mentioned guidelines have been satisfactorily applied in plenty of harbours (PIANC, 2015), when the problem has been detected and managed in due time. Still, it is very difficult to predict if a specific ship will induce great erosion due to the manoeuvres performed in a specific basin and the problem can only be detected by periodic inspection surveys. Moreover, the information in literature and the guidelines regarding the relationship between the ship manoeuvre characteristics and its effects over the seabed is scarce. Some standard situations are defined in (BAW, 2010), that consider, for instance, the distance from the ship to a vertical boundary or the presence of a rudder, but no general guidance including the manoeuvre pattern is present. In some communications, there is explicit mention of the most harmful manoeuvre situations. For instance, according to (Hawkswood et al., 2014), the most harmful manoeuvre section is the cast off, when the ship has no motion and accelerates to gain steerage. In their work, the authors also make explicit mention to the crabbing motion. They advise that no experimental studies are found in literature, but it is suspected that these specific manoeuvres may cause greater erosion depths. Crabbing is the ability of ships to move sideways without forward speed. In nautical terms it means that a specific ship has sway motion but no surge. This lateral motion is usually achieved by combining astern and ahead propellers with bow-thruster.

The present work uses the methodology applied in (Llull et al., 2020) in a case study, combining field data with a manoeuvre numerical simulator, to analyse the manoeuvre pattern and take the engine behaviour into consideration when studying the propeller-induced sediment scour at field. The field data consist of a series of annual bathymetric surveys performed at a specific harbour basin, where scour due to the manoeuvres of ferry ships was found. Moreover, AIS data is included to study and characterize the manoeuvre. AIS stands for Automatic Identification System and is defined in (IMO, 2003) as an automatic tracking system for identification and location of vessels by exchanging data via VHF communication to other nearby vessels (Castells et al., 2018). The manoeuvre is reproduced on a manoeuvre simulator, which allows to obtain the engine and bow thrusters behaviour, which is later triggered to the bed morphology evolution.

2. CASE STUDY

2.1. BACKGROUND OF THE STUDY

The present work arises from background studies performed at an inner basin of the Port of

Barcelona with significant problems related to ship propeller scour. This harbour basin has been traditionally used as large ferry ship berthing terminal. The research performed by (Mujal-Colilles et al., 2017) showed the evolution of the harbour basin from 2007 to 2014 (*Period 1* from this point in advance), while the work presented by (Castells et al., 2018) extended the analysis up to 2017 (*Period 2* from this point in advance). The work performed so far has been based on the analysis of the evolution of the basin morphology from bathymetric surveys performed by the Port Authority. In Figure 1, the evolution of the seabed morphology is observed through annual bathymetric surveys. During the *Period 1*, the berthing location of the study ship changed. In the previous years (2007-2012), the ferry ships berthed mostly at the North-Quay (Mujal-Colilles et al., 2017). The effects of these ships over the bottom material in the North-Quay (before 2012) are observable in the first bathymetry, which show scour holes reaching almost -18 m. Between 2012 and 2014, the ships berthed mostly in the West-Quay, which is the region of interest in the present work. In both Figure 1 and Figure 2, it is shown that between 2012 and 2014, the berthing ships created a scour hole in the new berth that reached again -18 m depth. The erosion pattern is also clearly defined, going from the West Quay – South Quay corner to the centre of the basin. Because of that, the Port Authority decided to perform adaptation works in 2015 (Port de Barcelona, 2015). The works consisted on the refilling of the affected regions with recycled material (20-300 mm) up to the -14.5 m level. After that, the refilling material was covered by a 1 m thick rock layer ($D_{50} \approx 0.5$ m), reaching therefore the -13.5 m level. The area of protection is shown with black contour lines in Figure 1, from 2015 on. After the adaptation works, the bed level was flattened (see Figure 2 profiles 2015, in red) in the centre of the basin. After the adaptation works, in 2017, new areas of erosion appeared in the surroundings of the protection patch (see Figure 1, 2017, and Figure 2, profile 3) with maximum depths reaching -16 m level. A part of the erosion, an accretion area is observed in 2014, that increases in 2015 and up to 2017, reducing the operational draught of the basin between 2014 and 2017 up to -8m (see Figure 2, profile 1), dangerously close to the maximum draught of the biggest ship operating in the basin, which is ~7m.

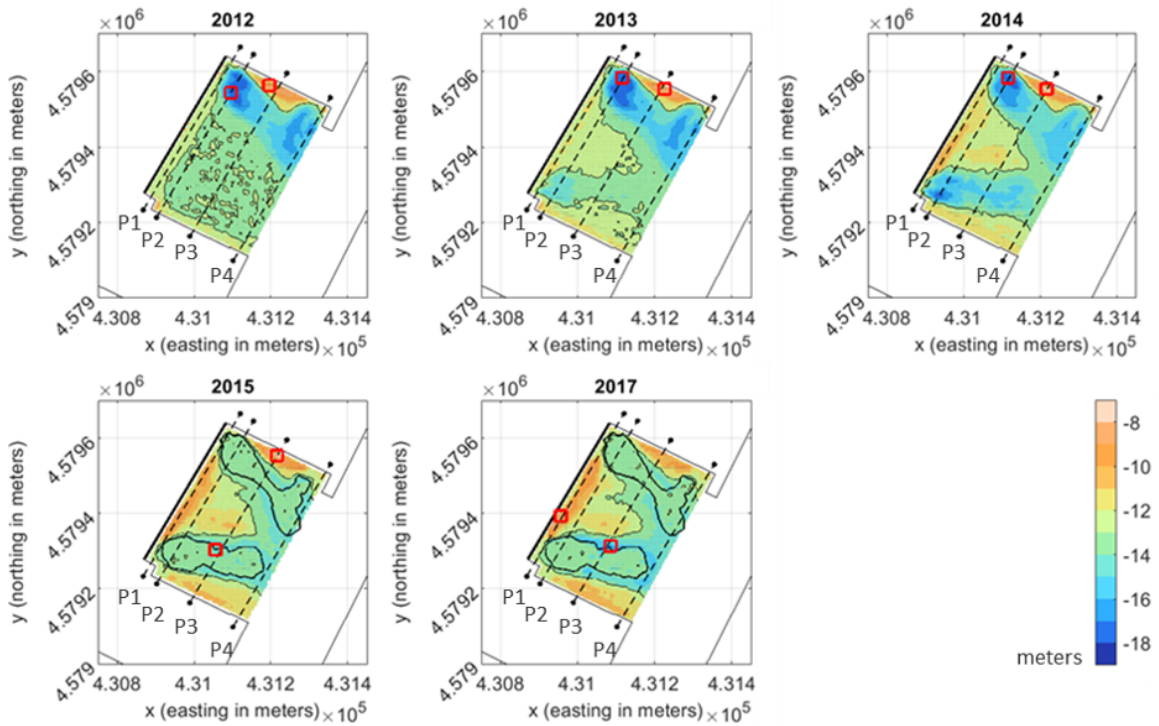


Figure 1. Bathymetric surveys at the study basin performed from 2012 to 2017 (Periods 1 and 2). The red squares (30x30m) show the location of the maximum erosion and accretion, averaged along the area of the square. The black solid line at the West-Quay shows the berthing location of the ferry during these time periods. The black polygon in the basin (from 2015) show the location of the protection patch. The black dashed lines show the different sections from which elevation profiles are obtained. The elevation profiles are here named as P1 to P4 (see Figure 2).

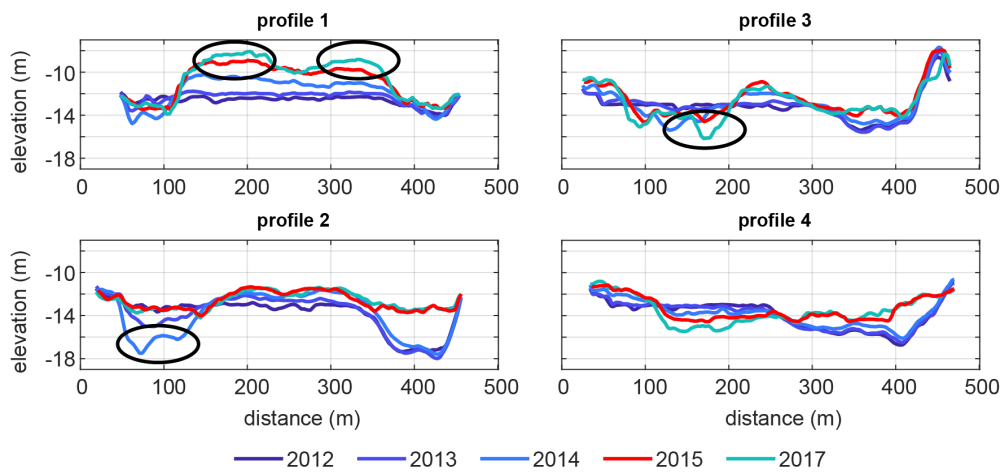


Figure 2. Elevation profiles 1 to 4 (from South to North in Figure 1), parallel to the West, between 2012 and 2017. The profile corresponding to 2015 is shown in red to highlight it, since it is taken from the bathymetries performed after the adaptation works in the basin. The black circles show the relevant areas of low or high depth.

2.2. RECENT EVOLUTION OF THE BOTTOM MORPHOLOGY

The evolution of the bathymetry of the harbour basin between 2018 (just after dredging operations in the central part of the basin) and 2021 is analysed from the data provided by the Port Authority. In Figure 3, an annual bathymetric survey shows that the erosion near the protection patch grows year by year and that a secondary erosion pattern appeared from 2019 from the West Quay – South Quay corner to the centre of the basin. The maximum erosion depth in 2021 is observed nearby the protection patch, reaching -18 m (see Figure 4, profiles 3 and 4), which is 5 m below the flattened level (see for instance Figure 4, profile 3). To clearly depict the evolution of the harbour basin, an erosion-accretion map is shown in Figure 5, in which the relative changes in depth between 2018 and 2021, i.e., the difference in depth at each 3x3 m grid of the whole basin between these years are observed. The time-series of erosion-accretion depth (at the markers location), areas and volumes indicate that the region below the protection patch has a clearly growing erosion trend, while the region nearby the West Quay clearly shows a constant reduction of the water depth, in this case at a lower rate. Interestingly, the evolution of volume of erosion and accretion material is similar, meaning that the basin keep the sediment balance. Therefore, although local erosion is observed, the eroded sediment settles nearby and does not leave the basin. Consequently, since the volume is kept constant but the erosion is greater than the accretion, the area of eroded material must be smaller than the area of accretion, as shown also in Figure 5(b).

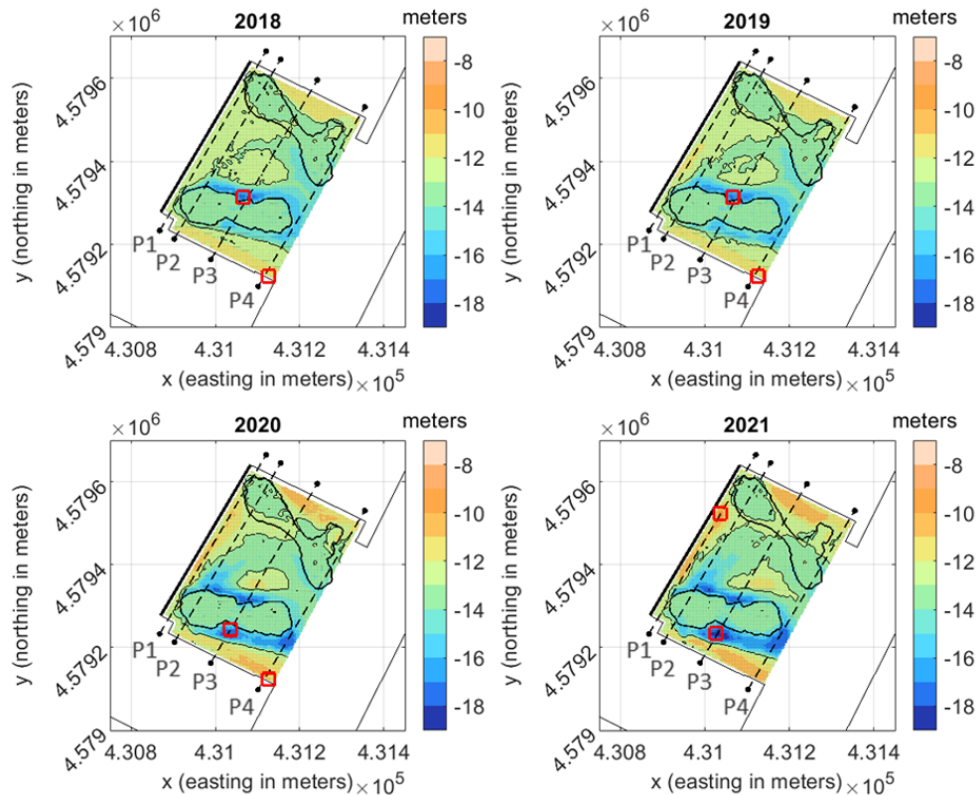


Figure 3. Bathymetric surveys at the study basin performed from 2018 to 2021. The red

squares (30x30m) show the location of the maximum erosion and accretion, averaged along the square area. The black solid line at the West-Quay shows the berthing location of the ferry during these time periods. Continuous thick black line after 2015 shows the location of the protection patch. The black dashed lines show the different sections from which elevation profiles are obtained. The elevation profiles are here named as P1 to P4 (see Figure 4).

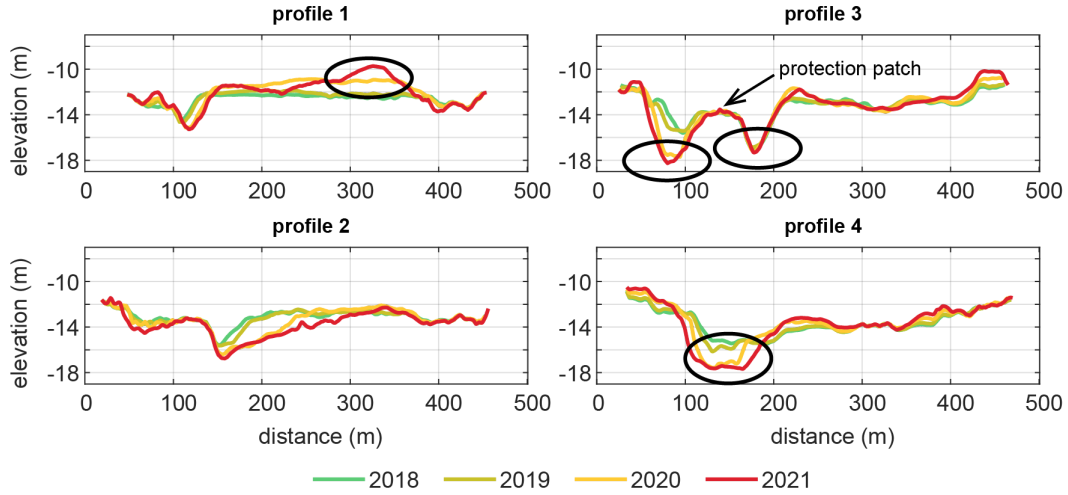


Figure 4. Elevation profiles 1 to 4 (from South to North in Figure 3), parallel to the West Quay, between 2018 and 2021. The areas of greater erosion/accretion are circled in black. Also, the area of protection patch, surrounded by great erosion is pointed in profile 3.

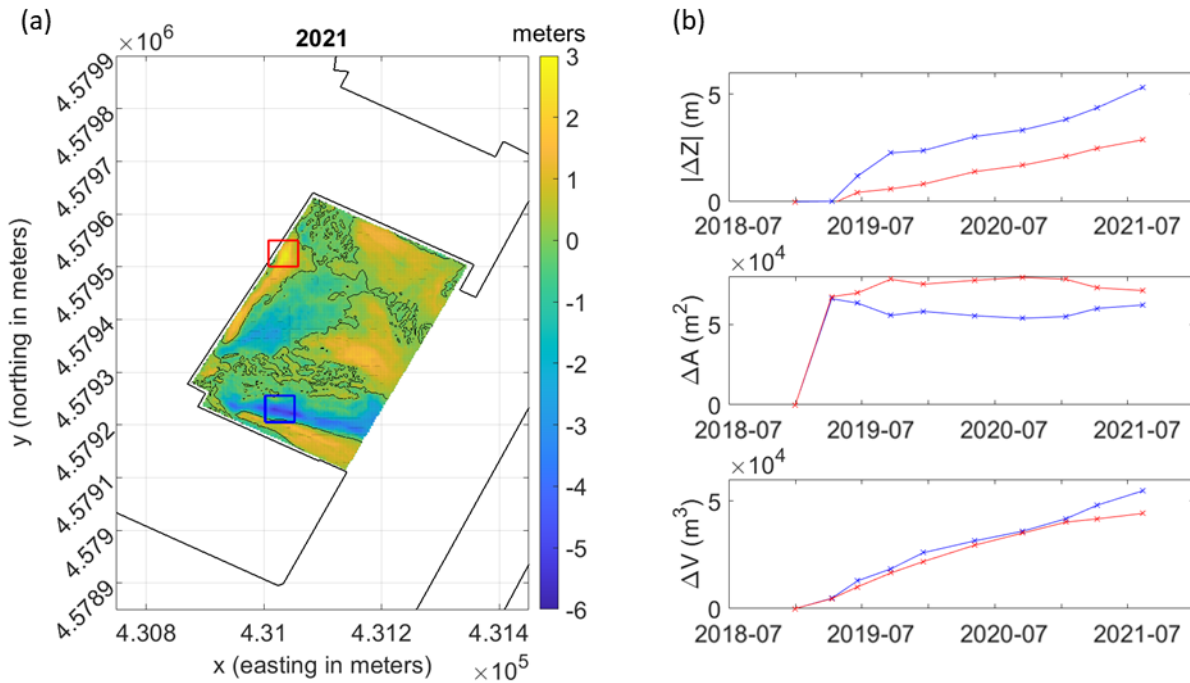


Figure 5. (a) Erosion-Accretion map from 2018 to 2021; (b) time-series of erosion and accretion in terms of depth (ΔZ), area (ΔA) and volume (ΔV).

3. METHODOLOGY

3.1. AIS DATA

An AIS transmitter was installed at the Barcelona School of Nautical Studies (FNB-UPC) to directly obtain AIS data from nearby ships. The system allows to directly receive AIS messages from all the ships in the surrounding area of Barcelona (up to 30 nautical miles, with a maximum range of 120 nautical miles, weather permitting). AIS data from September 2019 to July 2021 is used in this work to analyse the traffic in the study basin, identify vessels causing higher erosion in the basin, obtain a characteristic study vessel and analyse the manoeuvres the study vessel performs in the basin. The accuracy of the GPS position is expected to be approximately 8m, after test measurements with a signal at a fixed location (Bages Yañez, 2020).

3.2. MANOEUVRE SIMULATOR

The FNB-UPC hosts a Wärtsilä NTPro 5000-v-5.35 manoeuvre simulator designed to be used for Pilot and Captain training, in naval engineering and port management (see Figure 6). By using this simulator, the recorded manoeuvres from AIS messages are reproduced to obtain the specific behaviour of every necessary variable to estimate the propeller induced erosion over the bed. The georeferenced geometry of the port and the AIS data are inputs known in the simulator. To perform any manoeuvre in the simulator, the manoeuvre track is first introduced in the electronic nautical chart (ECDIS -Electronic Chart Display and Information System-) of the simulator to guide the user during the whole manoeuvre. Later, the manoeuvre is fully performed by a specialized operator and the output of the simulator is saved in a local disk. The output of the simulator contains important parameters related to the ship performance and the engines behaviour. The first are used to validate the manoeuvre, while the last are used to estimate the erosive action (see Table 1).

Table 1. Summary of the simulator output

	Variable	Units
Ship performance	Geographical position	Lat, Lon (degrees)
	Heading (HDG)	Degrees
	Speed Over Ground (SOG)	Knots
	Manoeuvre time	Seconds
Engines behaviour	Main Engine Power	kW
	Bow-thrusters Power	kW



Figure 6. Picture of the bridge of the manoeuvre simulator hosted by the FNB-UPC that was used to reproduce the manoeuvres in this work (Amengual Obrador, 2019).

3.3. LITERATURE EQUATIONS

From the output of the simulator, the existing formulae to characterize the efflux velocity (U_0) (Eq. (1)) and to estimate the magnitude of the maximum velocity at bed (U_b) can be applied. The computation of U_b depends on the method used and the combination of the ship location respect to the walls, the bed and the number of working propellers. In this work, two methods will be used to compute the velocity at bed, known in PIANC, (2015) guidelines as the Dutch and the German Method. Depending on the proximity of the propellers to the vertical walls, two different situations are considered: confined or unconfined conditions. In the first, the jet flow is deflected by the structures before reaching the bed. In the second, the jet spreads freely until it reaches the bed, without being deflected by any structure. Depending on the ship location and the engines use, different equations will be used in this work to compute U_b (see Eqs. (2-5)).

$$U_0 = C_1 \left(\frac{f_p P}{\rho_w D_p^2} \right)^{\frac{1}{3}} \quad (1)$$

With

U_0	Efflux velocity ($\text{m}\cdot\text{s}^{-1}$)
C_1	1.48 for non-ducted and 1.17 for ducted propellers (-)
f_p	Percentage of installed power used
P	Installed Power (kW)
ρ_w	Water density ($\text{kg}\cdot\text{m}^{-3}$)
D_p	Propeller diameter (m)

Confined	Dutch	$U_b = 2.8 U_0 \left(\frac{X_w + C_h}{D_p} \right)^{-1} \quad (2)$
----------	-------	---

	German	$U_b = 1.9 \alpha U_0 \left(\frac{X_w}{D_p} \right)^{-1} \quad (3)$
--	--------	--

	Dutch	$U_b = 0.216U_0 \left(\frac{C_h}{D_p} \right)^{-1} \sqrt{n}$	(4)
Unconfined	German	$U_b = C_2 U_0 \left(\frac{C_h}{D_p} \right)^{C_3}$	(5)

With

X_w	Wall clearance (m)
C_h	Bed clearance (m)
n	Number of working propellers (-)
U_b	Bed velocity ($\text{m}\cdot\text{s}^{-1}$)
C_2	0.71 for single propeller with central rudder and 0.52 for twin propellers with twin rudders (-)
C_3	-1 for single propeller and -0.275 for twin propellers (-)
\propto	Factor as a function of the wall and bottom distance (-)

The estimated U_b is one of the needed inputs to the equations used in bed protection design. For instance, in (Blokland and Smedes, 1996), Izbash criterium ($\beta_{is} > \beta_{is,cr}$) is used (Eq. (6)) to determine the bottom stability. In their work, Shields criterium ($\Psi < \Psi_{cr}$) is also used (Eq. (7)), after determining an empirical friction coefficient (C_f) based on the measured transport intensity. These methods will be used in the present work to assess the stability of two different grain sizes under the effect of the propeller jet loads. The grain sizes will be determined according to the information from the Port Authority about the bed protection used in the adaptation works (see Section 2) to test their suitability.

Izbash parameter	$\beta_{is} = \frac{2g\Delta D_{50}}{U_b^2}$	(6)
------------------	--	-----

Shields parameter	$\Psi = \frac{\tau}{\gamma\Delta D_{50}}$	(7)
-------------------	---	-----

	$\tau = \frac{1}{2}C_f\rho U_b^2$	(8)
--	-----------------------------------	-----

With

β_{is}	Izbash parameter (-)
g	Gravity ($\text{m}\cdot\text{s}^{-2}$)
Δ	Relative buoyant density (-)
D_{50}	Rock diameter (m)
Ψ	Shields parameter (-)
τ	Bed shear stress ($\text{N}\cdot\text{m}^{-2}$)
γ	Specific weight ($\text{N}\cdot\text{m}^{-3}$)
C_f	Friction coefficient (-)

4. RESULTS

4.1. AIS DATA IN THE HARBOUR BASIN

AIS data from 2019/09 to 2021/07 is obtained directly from the FNB-UPC AIS station and analysed in this work. Once the data is loaded, two datasets containing decoded AIS dynamic and semi-static messages are obtained. Due to the huge amount of accumulated data, 1-month files are made to pre-process the whole dataset with self-made script implemented in *MATLAB*® environment. An average month consist of ~7.7 million dynamic messages and ~500 000 semi-static messages. The headers of the obtained files are shown in Table 2.

Table 2. Information contained in the datasets of dynamic and semi-static messages.

Semi-static messages	Dynamic messages
Date-Time	Date-time
Message Type	Second sent
MMSI	MMSI
IMO	Status
Ship Name	Turn
Ship Type	Speed
Distance Bow	Longitude
Distance Stern	Latitude
Distance Port	Course
Distance Starboard	Heading
Draft	
Voyage	

The AIS dynamic and semi-static messages are not broadcasted at the same frequency. However, they can be easily linked through the MMSI indicator. In this case, unique combinations of time (rounded to 1/6 of hour) and MMSI numbers, are used to link each dynamic message with the interesting information in the semi-static messages: draft and distance from the AIS antenna to the vessel’s Port, Starboard, Bow and Stern.

The obtained datasets are then filtered by the area of interest. In this work, all the data outside the harbour basin and the attached navigation channel is removed. This region is limited by a 400 m radius between a central point in the study basin, located at position (41.3625, 2.1769) (see Figure 7). A speed filter is also included in the data-processing flow, with outliers considered as $SOG < 0.1$ kn & $SOG > 15$ kn. Velocities over 15 knots are not considered since the region of interest is an inner basin of the harbour, where SOG is limited to 7 knots. Once the data is filtered, a category is assigned to each message according to the geographical position contained in it. Depending on the point location, the message is considered to have “No error”, to be “Ground Data” or “Ground MMSI”. The first corresponds to messages containing a geographical position within the boundaries of the coast line; the second corresponds to messages containing positions that are located on the ground (0.31% of the data), and the third corresponds to messages whose MMSI and time (rounded to the hour) is coincident with one of the “ground data” messages. In Figure 7, the different AIS position coloured by category are shown for a 1-month period.

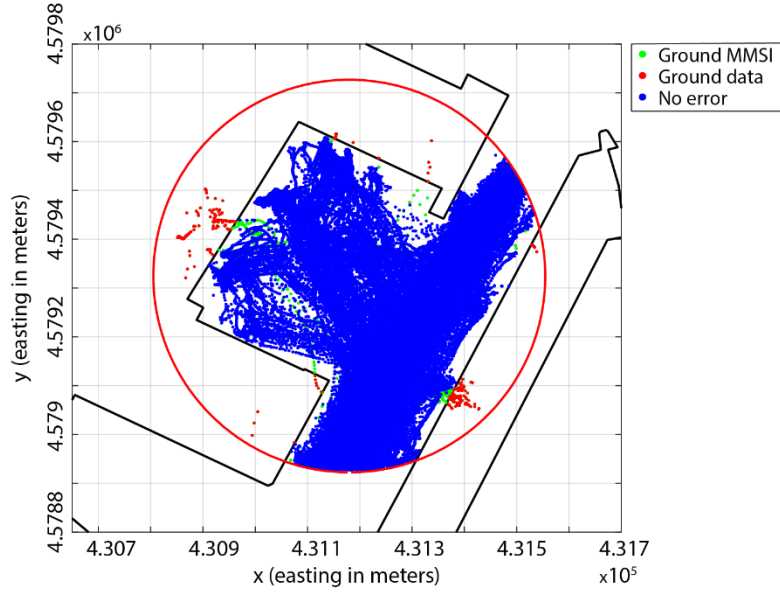


Figure 7. Example of 1-month period AIS data categorization (October 2019). The red circle shows the 400 m limit from the central point at position (41.3625, 2.1769).

To select the study vessel, the point density (histogram) of each unique ship manoeuvring in the basin is used. Confident results from the histogram are obtained when the data is time-interpolated with equally-spaced intervals. To do that, the start and the end of each track needs to be determined for each ship. Since the AIS broadcasting frequency rates are known (see Table 3), the start and end of each track is detected when the time interval between two consecutive messages for a unique ship is greater than 2 minutes.

Table 3. Broadcasting rates regarding the vessel's dynamic conditions as per ITU-R M.1371-5 recommendations

Dynamic conditions	Broadcasting rate (seconds)
At anchor / At berth with SOG < 3 kn	1800
At anchor / At berth with SOG > 3 kn	10
Underway using engine with SOG < 14 kn	10
Underway using engine with SOG < 14 kn and changing course	3.3
Underway using engine with 14 kn < SOG < 23 kn	6
Underway using engine with 14 kn < SOG < 23 kn and changing course	2
Underway using engine with SOG > 23 kn	2
Underway using engine with SOG > 23 kn and changing course	2

Once the data is interpolated (a sampling rate of 10s is used here), the SOG can be computed at each time-step as the ratio between the distance from to consecutive points and time. The AIS data is shown in Figure 8, coloured by SOG and corresponding to the period

from September to December 2019.

Considering only the inner basin (see Figure 8), the histogram of positions of vessels yields the most common manoeuvring vessel (see Figure 9). Moreover, the size of the ships in the inner basin is also analysed, yielding that the most common ships in the basin are also the second bigger among all the ships recorded in the basin since September 2019 (Figure 9). Based on the former, the mentioned vessels, which are sister ships, are selected as the study ship of this work.

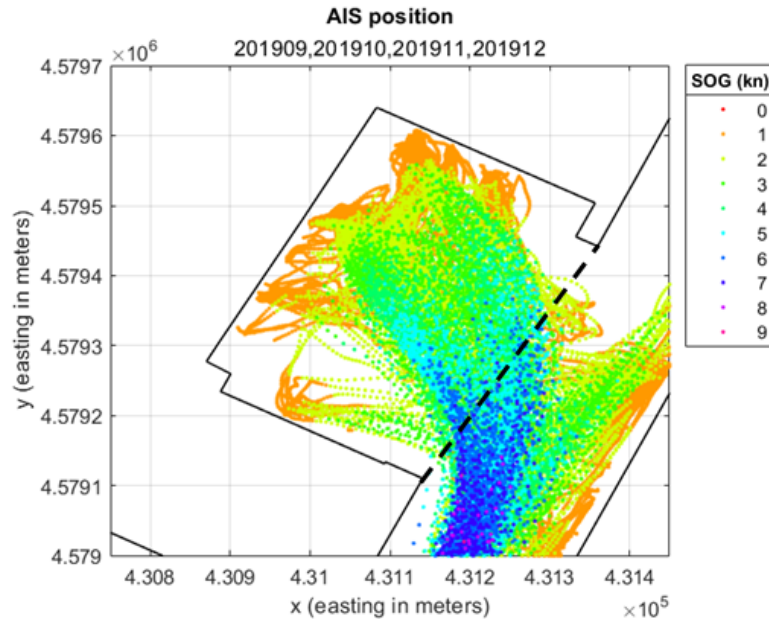


Figure 8. Interpolated AIS data at $\Delta t = 10$ s, coloured by SOG. Data corresponding to the period between September and December 2019. The dashed line shows the division between the inner-basin and the navigation channel.

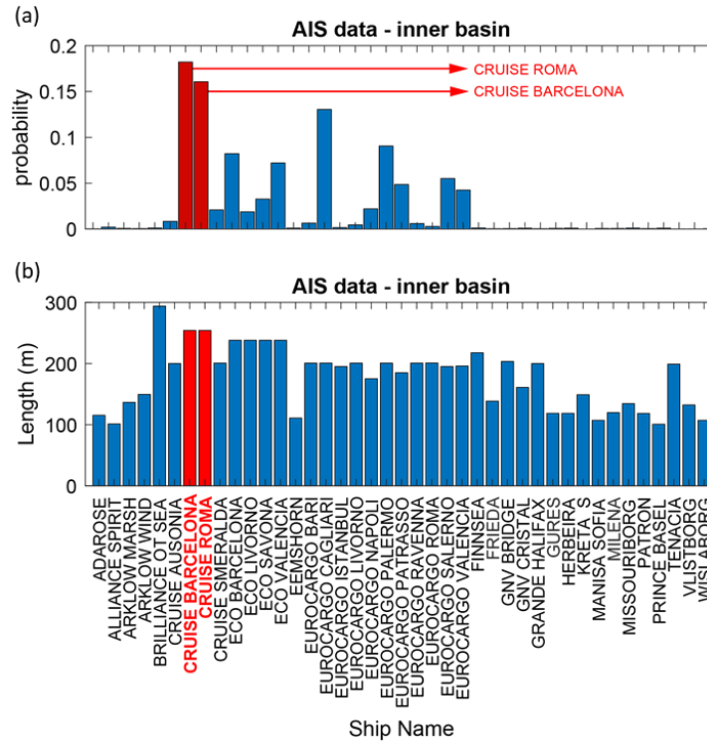


Figure 9. Use of the inner basin from AIS data between September 2019 and July 2021. (a) Probability of appearance of each ship in the inner basin; (b) Bar-plot of the lengths of each ship in the inner basin.

The study ship is a common Ro-Pax ferry ship which covers the route between Genova and Barcelona and scales 3 times per week in the area of interest of the Barcelona Port (see Figure 10). The characteristics of the study ship need to be compared with the characteristics of the simulator ship, which is chosen accordingly to get the maximum similarities. Table 4 shows a comparison between the main particulars of both ships, which are the same ship-type and have the same number of engines and propellers.

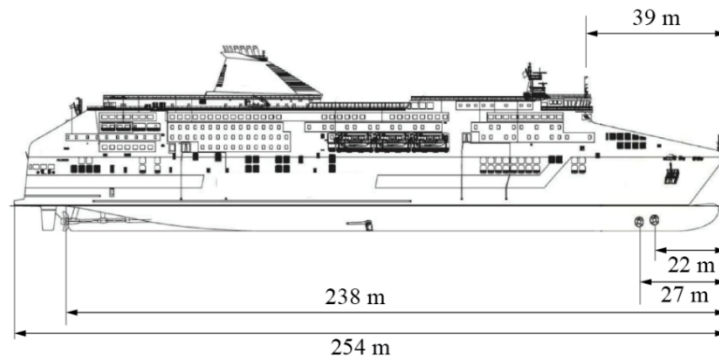


Figure 10. Sketch of the study ship showing some dimensions of interest: length overall, distance to the bow-thrusters, distance to the main propellers and distance to the AIS antenna.

Table 4. Main characteristics of the study ship and the simulator ship.

	Study Ship	Simulator Ship
Length overall (m)	254	196
Draught (m)	7.2	6.1
Breadth Moulded (m)	30.4	25
Main Engine Power (kW)	4 x 13860	50400
Number of main propellers	2	2
Type of propellers	CPP	CPP
Bow-thrusters Power (kW)?	2 x 1850	3400
Propellers immersion (m)	-	3.8
Propellers Diameter (m)	6	-
Bow-thrusters diameter (m)	2	-

4.2. MANOEUVRES OF THE STUDY SHIP

Once the study ship is determined, the whole AIS data-set is filtered and the manoeuvres of the study ship are isolated. In Figure 11, for instance, some randomly selected manoeuvres of the study ship are plotted. Not all of them are included due to the huge amount of data, which would lead to overlapping many ship's track lines. In this figure, the manoeuvre is split into three different sections that allow a first analysis of the manoeuvre. In case of the Arrival manoeuvre (A), the Manoeuvre Sections (MS) 1, 2 and 3 are identified and named MS1A, MS2A and MS3A. In the same way, the three Manoeuvre Sections of the Departure manoeuvre (D) are named MS1D, MS2D and MS3D. In the Arrival manoeuvre, MS1A is the approach to the harbour basin, MS2A is the approach to the berthing quay and MS3A is the final berthing phase, characterized by the lateral motion of the ship, in parallel to the side quay (crabbing motion). On the other hand, in the Departure manoeuvre, MS1D is the crabbing of the ship, in parallel to the side quay and moving away, MS2D is the starboard turn and MS3D is the final departure from the basin. This Manoeuvre Sections will be used from this point to analyse the whole manoeuvre both from the AIS data and, once the manoeuvre is reproduced, in the simulator.

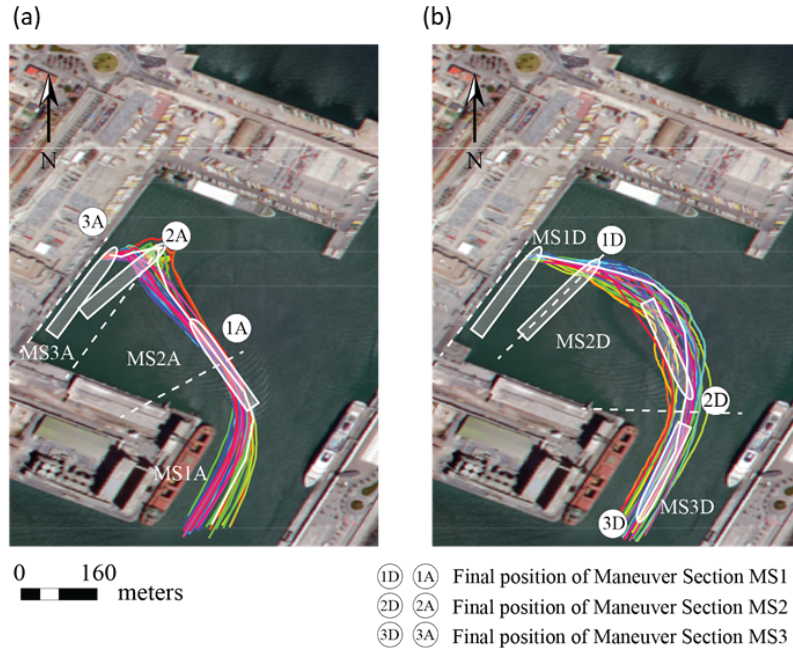


Figure 11. Example of ship's track lines of Arrival (a) and Departure (b) manoeuvres showing the three Manoeuvre Sections (MS) defined.

4.3. EROSION PATTERN DUE TO MAIN PROPELLERS LOAD

From the AIS data we obtain the mean manoeuvre and the position of the propellers. The position of the propellers is obtained by combining the AIS position, the ship's heading and the distance between the AIS transmitter to the ship's stern. The last information is part of the semi-static messages (see Table 2). The coincidence between the main propellers' location during the manoeuvre of the study vessel and the erosion pattern is clearly mapped in Figure 12, where the mean manoeuvre is superimposed to the last bathymetry (2021, see Section 2.2).

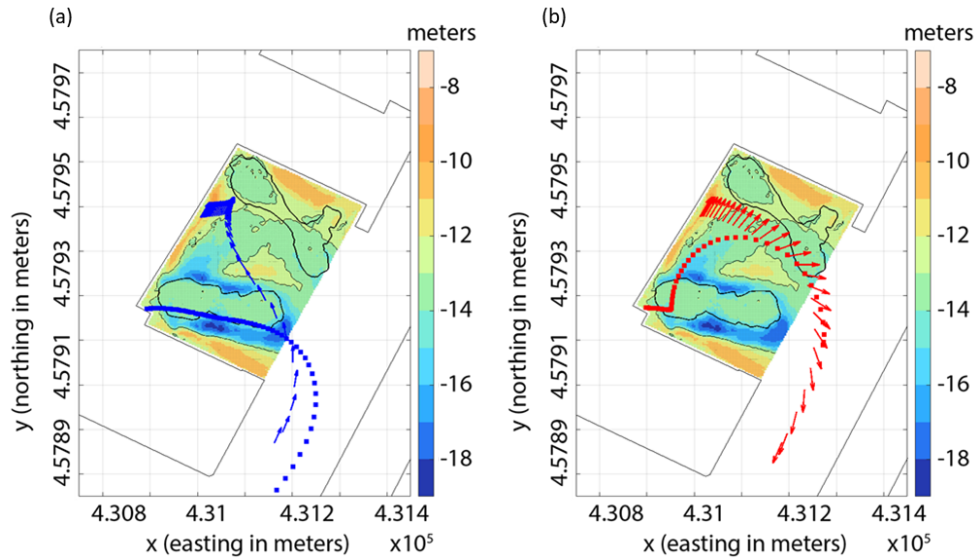


Figure 12. Mean manoeuvre from AIS data. (a) Arrival manoeuvre, (b) Departure manoeuvre. The AIS location is shown by heading arrows, which also point to the ship's heading. The approximate location of the main propellers is shown with solid squared markers.

4.4. MANOEUVRE SIMULATION AND VALIDATION THROUGH AIS DATA

Once the mean manoeuvre has been analysed from the AIS data, it is reproduced in the manoeuvre simulator. To reproduce the Arrival manoeuvre, the ship's bow heads to its final location near the berth, diminishing the speed from ~ 6 to ~ 1 knot. Once the ship is in the adequate location at low speed, a turning moment is induced to approach the ship's stern to the side-quay by combining ahead port and astern starboard engine orders. To avoid extra separation of the ship's bow from the side-quay, the bow-thruster may be used according to the manoeuvre requirements. Once the ship is in parallel to the side-quay and nearby, some final adjustment may be required to fit the final position by running the engines at very low regime. In the case of the Departure manoeuvre, the ship is moved away from the berth by using the bow-thruster outwards. The bow-thruster allows the separation of the ship, but also inducing a turning moment that needs to be compensated to prevent the stern from colliding with the dock. This is performed by combining astern port and starboard ahead engine orders. With this main engines / bow-thrusters combination, the ship describes a lateral motion away and in parallel to the side quay. Once the ship is safe, the main engines order is inverted, allowing the ship to perform a fast-starboard turn. As the turning is performed, the bow-thrust is reduced and the engines orders are progressively equated. Finally, once the ship is in the departure heading, both propellers run ahead and the ship departs the basin.

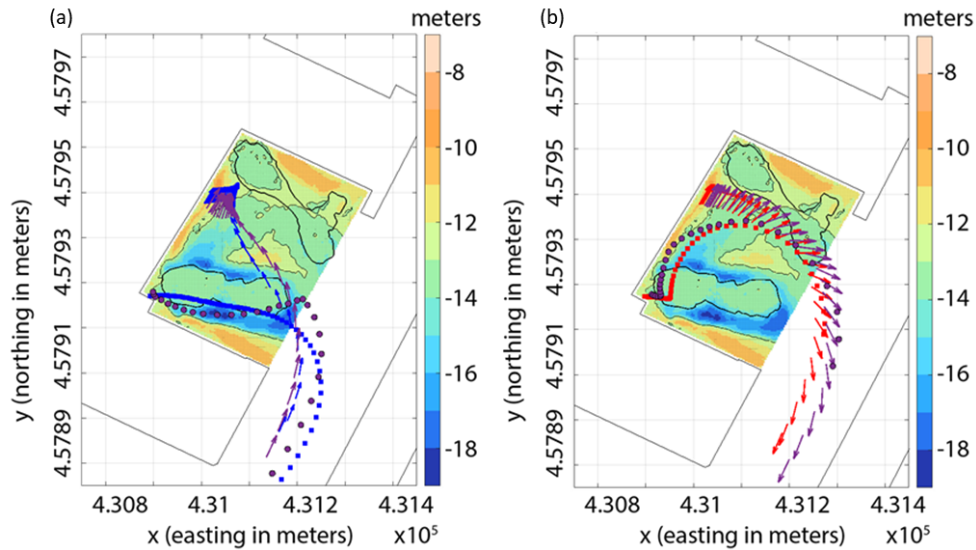


Figure 13. Mean manoeuvre from AIS data (blue in (a) Arrival and red in (b) Departure) compared with the simulated manoeuvre (purple). The manoeuvres are mapped over the last bathymetry of 2021.

To smoothly perform these manoeuvres, several tests are needed until the simulator instructor gets enough practice to perform the whole manoeuvre in time and following the real track. At this point, it may be interesting recalling that, in real conditions, the manoeuvre is performed by experienced Captains and Pilots with years of practice, so the specific manoeuvres they perform are usually difficult to mimic in the simulator. Each manoeuvre is accepted or discarded according to the simulator instructor's advice, the manoeuvre mapping as in Figure 13 and a further validation by comparing the time-series of the descriptors: SOG and HDG as in Lull et al., (2020) (see Figure 14).

Once a set of simulated manoeuvres is got, the mean manoeuvre from the simulator is obtained by ensemble averaging the time-series of the manoeuvre descriptors. The time-series of the mean manoeuvre from the simulator are compared with the AIS, as shown in Figure 14. The simulator time-series show very good agreement with the mean manoeuvre time-series obtained from the AIS data, thus validating the simulator manoeuvre and allowing the further analysis of the engines and propellers behaviour.

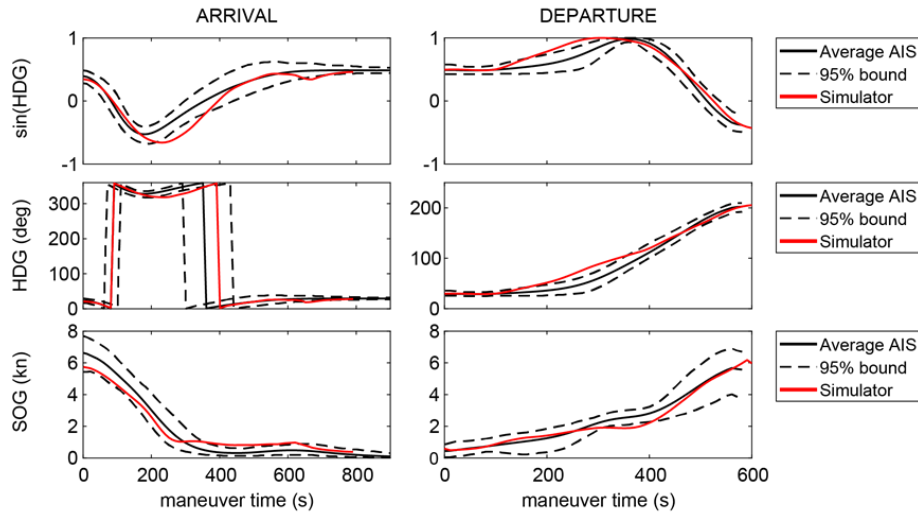


Figure 14. Time-series of Heading (HDG) and Speed Over Ground (SOG) of the mean manoeuvre both from AIS (black lines) and from the simulator (red lines).

4.5. OUTPUT OF THE SIMULATOR

The output of the simulator is analysed according to each Manoeuvre Section (MS) defined in Section 4.2 and plotted in the maps in Figure 15 to better depict the relation between the use of the engines and the effects over the bottom morphology. Particularly, the areas with greater erosion correspond to the MS2A and MS2D, with higher affectation due to the Arrival one. From the simulator output (Figure 16), it is observed that the higher engine power is used at the manoeuvre section MS2A, with an average engine order close to the 50% both ahead and astern (between slow to half ahead and astern). In comparison, during MS2D, the engine order varies between Dead Slow and Slow Astern and Ahead. Close to the quay-wall, in MS1D and MS3A, a similar engine behaviour is observed both in the Departure and the Arrival manoeuvres. At this Manoeuvre Section, the ship is close to the wall and it is assumed that the propeller jet is in a confined scenario. Still, the engine runs in this Manoeuvre Section at low regimes and, very close to the wall, only Dead Slow engine orders are expected to avoid uncontrollable situations due to sudden acceleration. Therefore, although the effect of the wall is known to increase the erosive potential of a propeller jet, the fact that lower engine regimes are expected near the wall implies that lower loads occurs at the quay toe.

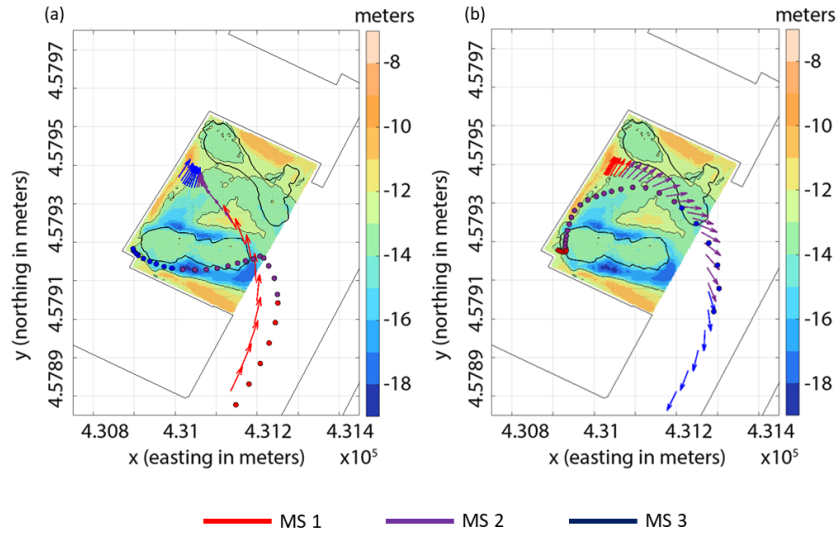


Figure 15. Simulator obtained manoeuvres coloured by Manoeuvre Section (MS) in case of (a) Arrival manoeuvre and (b) Departure manoeuvre.

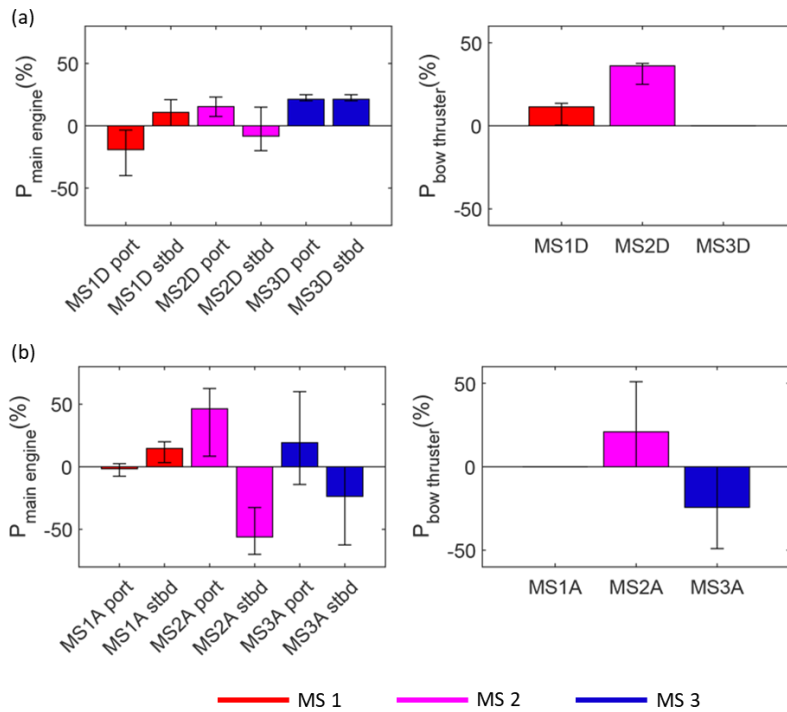


Figure 16. Simulator output showing the percentage of main engine power and bow thruster power used at each manoeuvre section in case of (a) Departure and (b) Arrival manoeuvre. The mean value is obtained as the average value of each manoeuvre section in the ensemble manoeuvre, while the error bands show the 5 and 95 percentile of the data in each section.

4.6. SCOUR PROTECTION ASSESSMENT

The results shown in the previous section are now used to compute interesting parameters to perform the erosion assessment based on the equations presented in Section 3.3. In

Figure 17 the results obtained are shown through bar-plots, coloured by MS. The efflux velocity (U_0) is first computed for the ahead rotating propellers. At this point, the backwards rotating propellers cannot be included since no recommendations are found in the guidelines to compute the velocity field in these cases. From the U_0 , U_b is computed with Eqs. (2-5). The computed flow velocities show differences depending on the method. According to (PIANC, 2015) the reason for the differences is that the German approach is based on a thorough research of all aspects: from the outflow via the flow velocities to the size of the bed protection. The Dutch approach aims at developing a method to predict the required stone size. The results obtained with the Dutch method will be used here to compute the stability of the erosion protection in the basin (see Section 2.1) both with Eq. (6) and Eq. (7).

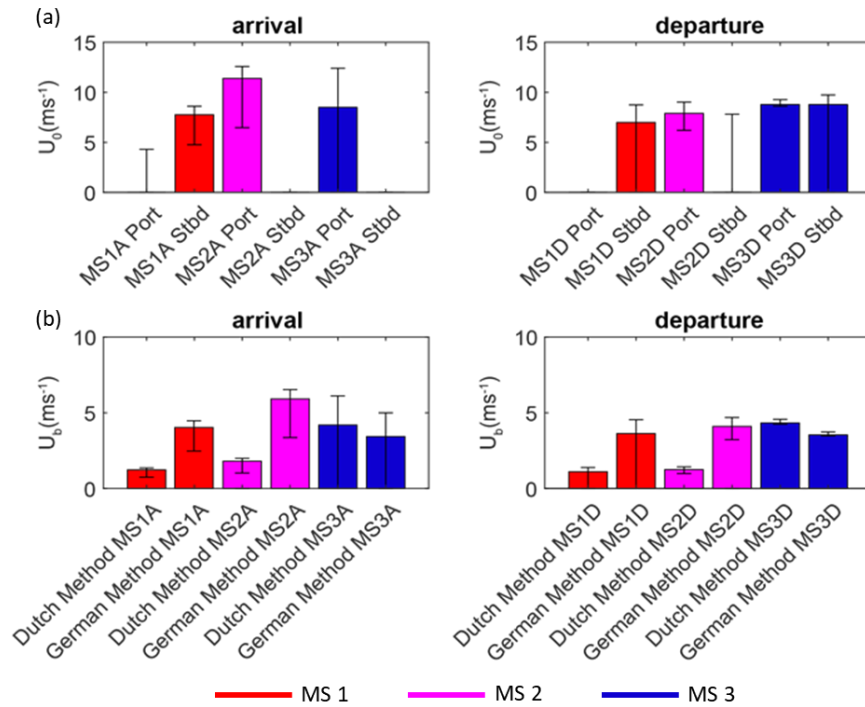


Figure 17. (a) Efflux velocity (U_0) and (b) bed velocity (U_b) computed from the simulator output with the equations in Section 2.3.

The results obtained from MS2A are coincident with the area of greater erosion and with the location of the protection patch (see Figure 15). Based on the information provided by the Port Authority about the rock size used in the protection patch (see Section 2.1), two characteristic diameters are used here: $D_{50} = 0.16$ m and $D_{50} = 0.55$ m, with density $\rho_s = 2600$ kg·m⁻³. To determine the bottom stability, Izbash and Shields criterium are used (see Section 3.3), where the critical Izbash and Shields parameter are $\beta_{is,cr} = 6$ and $\Psi_{cr} = 0.03$, respectively. The stability of the rock layer is determined using the values of the minimum, mean and maximum bed velocities as previously computed, considering the rock stability when $\beta_{is,cr} > 6$ and $\Psi_{cr} < 0.03$. The results are summarized in Table 5, showing that the refilling material is only stable under minimum flow velocities, while the

rock layer is stable even if the maximum bed velocity is used. The observed results in the bathymetric surveys show agreement with this statement, since the erosion is observed everywhere surrounding the protection patch, although the patch itself remains stable (see Section 2.2).

Table 5. Results of the bottom stability assessment based on two stability criteria for two different rock sizes. Green and red values show, respectively, stable and unstable rock diameters under the corresponding flow velocity.

D₅₀ = 160 mm	U₀	U_b (Dutch)	β_{is}	Ψ
Min	6	0.8	7.2	0.02
Mean	11	1.5	2.1	0.06
Max	12	1.6	1.8	0.07
D₅₀ = 0.55 m	U₀	U_b (Dutch)	β_{is}	Ψ
Min	6	0.8	27	0.005
Mean	11	1.5	8	0.016
Max	12	1.6	6.7	0.02

5. CONCLUSIONS

The present work used the methodology published in (Llull et al., 2020) to analyse a case study and link the erosion observed in a harbour basin to the manoeuvre pattern. The AIS information is clue to clearly visualize and define the manoeuvres sections and patterns. The AIS equipment now hosted by the FNB-UPC is an excellent tool to monitor manoeuvres of interest, compute manoeuvre time, extract statistics of harbour use, traffic, etc. In this particular case, the detail provided by the AIS system is enough to obtain a clear track of any manoeuvre that is willing to be studied. By using the manoeuvre simulator, evidence of the main characteristics of the main engines and bow thrusters performance during the arrival and departure manoeuvre is provided. The results obtained from the simulator are used as input to the main equations in literature to compute the flow velocity and the bottom stability.

The arrival manoeuvre is proven to be more harmful than the departure one in the harbour basin area under unconfined jet flow action. The coincidence in the scour pattern, obtained from the bathymetries of the harbour basin and the propellers location, yielded consistent results in this direction. After the use of the manoeuvre simulator, the results confirmed that higher engine power is needed to perform the arrival manoeuvre. Moreover, the regime of the main propellers during the whole manoeuvre is a combination of ahead and astern regime. The effects of the propeller jets in astern regime are not considered by the guidelines, but is expected to be important as per the presented results. Since the main scour pattern is in coincidence with the ship positions where both ahead and astern orders are needed, the estimation of the loads induced by astern rotating propellers is needed.

The use of the simulator allowed to obtain important parameters that are needed inputs to

the equations to compute the diameter of rock protection to ensure the bottom stability. The value of these parameters varies during the whole manoeuvre and therefore, by using the simulator, the study is adapted to a particular case. As per the observed results, although the protection patch in the basin is stable, great erosion areas are growing in its surroundings that may require rehabilitation works. Moreover, a new erosion pattern following the Departure manoeuvre track is observed. In the future, attention must be paid to the ship manoeuvre pattern to design erosion protected areas in harbour basins.

6. REFERENCES

1. Amengual Obrador, S. Proposta de maniobres alternatives per tal de minimitzar l'erosió en el Moll del Morrot (Port de Barcelona) [online]. Universitat Politècnica de Catalunya, Facultat de Nàutica de Barcelona. Departament de Ciència i Enginyeria Nàutiques, 2019.
2. Bages Yañez, C. Ús de les dades massives AIS com a eina de gestió poertuària [online]. Master thesis, Universitat Politècnica de Catalunya, Departament d'Enginyeria Civil i Ambiental, 2020. [Accessed: 16 June 2022]. Available at: < <http://hdl.handle.net/2117/334174> >
3. Bundesanstalt für Wasserbau. Principles for the design of bank and bottom protection for inland waterways (GBB). *BAW Codes of Practice and Guidelines* [online]. Karlsruhe, Germany: BAW, 2011. Issue 2010. ISSN 2192-9807. [Accessed: 16 June 2022]. Available at: < https://izw.baw.de/publikationen/merkblaetter/0/BAWCodeofPractice_Principles_Bank_Bottom_Protection_Inland_Waterways_GBB_2010.pdf >
4. Blokland, T.; Smedes, R.H. In situ tests of current velocities and stone movements caused by a propeller jet against a vertical quay wall. In: 11th International Harbour Congress: Antwerp, 17-21 June 1996. General Reports. Antwerp, Belgium: Koninklijke Vlaamse Ingenieursvereniging, 1996. ISBN 9052040303
5. Castells, M.; Mujal-Colilles, A.; Llull, T.; Gironella, F.X.; Martínez de Osés, F.X.; Martín, A.; Sanchez-Arcilla, A. Ship manoeuvre patterns to prevent propeller scouring effects. In: 34th PIANC World Congress, Panama 2018 May 7 to 11: Connecting Maritime Hubs Globally. *34th PIANC World Congress Book of abstracts*. World Association for Waterborne Transport Infrastructure (PIANC), 2018. ISBN 9782872232512. [Accessed: 16 June 2022]. Available at: < <http://hdl.handle.net/2117/131225> >
6. Hawkswood, M.G.; Lafeber, F.H.; Hawkswood, G.M.; Berth scour protection for modern vessels. In: PIANC World Congress San Francisco USA 2014. *Proceedings 33th PIANC World Congress* [online]. [Accessed: 16 June 2022]. Available at: < <https://proserveltd.co.uk/wp-content/uploads/2020/08/2014-Paper-Berth-Scour-Protection-for-Modern-Vessels.pdf> >
7. International Maritime Organization. *Guidelines for the onboard operational use of shipborne Automatic Identification System (AIS) Resolution*. IMO, 2003.
8. Llull, T.; Mujal Colilles, A.; Castells, M.; Gironella, X. Composite methodology to prevent ship propeller erosion. *Ocean Engineering*. January 2020, vol. 195, 106751. [Accessed: 16 June 2022]. Available at: <

- <https://doi.org/10.1016/j.oceaneng.2019.106751> >
9. Mujal Colilles, A.; Gironella, X.; Sanchez Arcilla, A.; Puig Polo, C.; Garcia Leon, M. Erosion caused by propeller jets in a low energy harbour basin. *Journal of Hydraulic Research* [online]. 2017, vol. 55, no. 1, p. 121–128. [Accessed: 16 June 2022]. Available at: < <https://doi.org/10.1080/00221686.2016.1252801> >
 10. The World Association for Waterborne Transport Infrastructure (PIANC). Guidelines for protecting berthing structures from scour caused by ships. *PIANC Report*. PIANC. 2015, Repor no. WG180.
 11. Port de Barcelona. *Annual Report 2015* [online]. Barcelona: Port de Barcelona, 2016. [Accessed: 16 June 2022]. Available at: < https://contentv5.portdebarcelona.cat/cntmng/guestDownload/direct/workspace/SpacesStore/46232079-0698-4d3f-bf7c-0df03150b5c2/2015_PortBCN_en.pdf >
 12. Puertos del Estado. *Obras de atraque y amarre: Criterios generales y Factores del Proyecto: R.O.M. 2.0-11*. Gobierno de España, Ministerio de Fomento, 2012. [Accessed: 17 June 2022]. Available at: < <https://www.puertos.es/es-es/BibliotecaV2/ROM%202.0-11.pdf> >.

1.